Divergent functional and conformational outcomes in an ion channel-peptide interaction

Christian B. Borg[#], Stephanie A. Heusser[#], Janne M. Colding, Stephan A. Pless*

Center for Biopharmaceuticals, Department of Drug Design and Pharmacology, University of Copenhagen, 2100 Copenhagen, Denmark

[#] Contributed equally

* Corresponding author:

Stephan Pless

Center for Biopharmaceuticals

Department of Drug Design and Pharmacology

University of Copenhagen

Jagtvej 160, 2100 Copenhagen, Denmark

Mail: stephan.pless@sund.ku.dk

Abstract

Acid-sensing ion channels (ASICs) are trimeric proton-gated cation channels that contribute to fast synaptic transmission. Pharmacological inhibition of ASIC1a has been shown to reduce neurotoxicity and infarct volumes during stroke. The cysteine knot toxin Psalmotoxin-1 (PcTx1) is one of the most potent and selective inhibitors of ASIC1a. PcTx1 binds at the subunit interface, but both the stoichiometric requirements and the dynamics of the conformational consequences of the ion channel-peptide interaction remain unknown. Here, we use a combination of electrophysiology, voltage-clamp fluorometry and subunit concatenation to decipher the mechanism of PcTx1 inhibition. We observe a long-lived PcTx1-induced conformational change in the ASIC1a extracellular domain that is destabilized by the F350L mutation at the PcTx1 binding site. Concatemeric channel constructs show that two WT ASIC1a subunits are sufficient for WT-like current inhibition, while the presence of a single mutated subunit is enough to destabilize the PcTx1-induced conformation. Our results therefore demonstrate a divergence between the functional effects of PcTx1 on the pore and its conformational consequences in the extracellular domain. It further highlights how engineering of ion channels enables precise control over individual subunits for pharmacological and conformational assessment to determine the mechanism of ion channel–ligand interactions.

Introduction

Acid-sensing ion channels (ASICs) are trimeric proton-gated cation channels expressed throughout the central and peripheral nervous system (Gründer 2020). The extracellular domains (ECDs) of ASICs sense pH changes, allowing cations to permeate through the channel pore comprised of the transmembrane domain (TMD) (Figure 1A). Research over the last two decades has shown that this pH-activated current underlies various physiological processes, such as fast synaptic transmission (Du, Reznikov et al. 2014), learning and memory (Wemmie, Chen et al. 2002). More recently, ASICs have emerged as a potential drug target in neurological diseases, following reports of ASIC1a inhibition exhibiting neuroprotective effects, including protection from acidosis-induced neurotoxicity and reduction of infarct volume in mouse models. (Xiong, Zhu et al. 2004, Wemmie, Taugher et al. 2013, Chassagnon, McCarthy et al. 2017, Qiang, Dong et al. 2018, Gründer 2020).

ASICs exhibit a rich pharmacology with highly complex molecular details. Modulators can affect activation, steady-state desensitization (SSD)—a state reached at sub-activating proton concentrations that reduces subsequent activation—but also metabotropic downstream signalling (Kellenberger and Schild 2015). Venom-derived peptides are currently the most selective and potent modulators of ASIC1 and therefore serve as valuable tools to gain deeper insights into the mechanisms of ASIC modulation (Cristofori-Armstrong and Rash 2017). Psalmotoxin-1 (PcTx1) is a 40-residue cysteine knot peptide toxin extracted from tarantula venom (Escoubas, De Weille et al. 2000). It acts as a potent gating modifier of channels containing ASIC1 subunits (Chen, Kalbacher et al. 2005, Chen, Kalbacher et al. 2006). It shifts activation and SSD curves to more alkaline values and thereby effectively inhibits the channel in the low nanomolar range at neutral pH (Cristofori-Armstrong and Rash 2017). Mutation of F352 (F350 in mASIC1a) to either alanine or leucine, however, significantly attenuate the PcTx1 effect on ASIC1a channels (Sherwood, Franke et al. 2009, Saez, Deplazes et al. 2015). Further species-, gating- and ion-dependent factors can greatly influence the functional outcome of PcTx1 modulation (Sherwood, Lee et al. 2011, Cristofori-Armstrong, Saez et al. 2019), yet little is known about the conformational consequences of the interaction in different functional states and under varying pH conditions.

Structural studies have shown that PcTx1 binds to the subunit interfaces of cASIC1, forming contact points with the primary and complementary side of the acidic pocket (Dawson, Benz et al. 2012, Baconguis, Bohlen et al. 2014) (Figure 1A). However, it remains unclear how many toxin molecules are required to obtain functional channel modulation. Conventional approaches are inapt to answer this fundamental question as it is technically impossible to introduce targeted mutation in a single subunit within a homotrimer, and coexpression of non-concatenated WT and mutant subunits may lead to undesired, heterogeneous subunit assemblies precluding accurate interpretation of functional data. The use of concatemeric constructs helps to overcome these limitations. By fusing cDNAs of subunits of interest in the desired order, this approach predetermines the subunit composition and assembly of channels, allowing us to directly address questions such as the number of PcTx1 binding sites needed for functional inhibition. Importantly, the trimeric assembly ASICs has proven to be highly amenable to this approach (Joeres, Augustinowski et al. 2016, Lynagh, Flood et al. 2017, Wu, Chen et al. 2019).

To decipher the stoichiometric requirements for the functional and conformational consequences of the PcTx1-ASIC1a interaction, we designed concatemeric mASIC1a constructs carrying the F350L substitution in one, two, or all three subunits. We combined this approach with electrophysiological and voltage-clamp fluorometry experiments to gain insight into conformational changes induced by PcTx1 binding and unbinding. Our results illustrate that at neutral pH, two intact PcTx1 binding sites are sufficient for WT-like functional inhibition. By contrast, our voltage-clamp fluorometry recordings reveal a distinct PcTx1-induced conformational state that is destabilized even by a single F350L-containing subunit. These results highlight how engineered channels allow us to efficiently control subunit composition and simultaneously follow conformational changes related to gating and toxin modulation. This enabled us to provide insight into the complex pH-dependent conformational changes induced by PcTx1, decipher the stoichiometry of toxin binding and uncover a partial uncoupling of the extracellular conformation from the state of the pore that was not predicted by previous structural or functional studies.

Results

F350L mutation drastically diminishes PcTx1 sensitivity

First, we sought to determine the PcTx1 sensitivity of WT ASIC1a and compare it to that of a mutation that renders the channel virtually insensitive to the toxin (Sherwood, Franke et al. 2009, Saez, Deplazes et al. 2015). To this end, we expressed WT and F350L mASIC1a in *Xenopus laevis* oocytes and applied PcTx1 at a pH value that would neither activate nor steady-state desensitize the channels in the absence of the toxin (pH 7.9 for WT; pH 7.6 for F350L). At pH 7.9, 30 nM PcTx1 led to a shift of the activation curve of mASIC1a WT over 0.5 pH units to more alkaline values (Figure 1B, D; Table S1). Additionally, PcTx1 also affected ASIC1a SSD, causing an alkaline shift of the pH_{50_SSD} by 0.4 pH units (Figure 1C, D; Table S1). Consistent with previous findings (Sherwood, Franke et al. 2009), introducing the F350L mutation reduced the pH sensitivity of activation and SSD (Figure 1E; Table S1). The presence of 30 nM PcTx1 only led to a slight shift in pH_{50_SSD} but had no effect on channel activation (Figure 1E; Table S1). We therefore wanted to establish the potency of PcTx1 at physiological pH (7.4) on subsequent pH 5.6 activation in the F350L variant compared to WT (Figure 1F). In WT, PcTx1 displayed an IC_{50} of around 0.6 nM (Figure 1F,G; Table S2). The F350L variant was still inhibited by PcTx1 in a concentration-dependent manner, yet compared to WT, the PcTx1 sensitivity of the F350L mutant was dramatically decreased to an IC_{50} of around 1 µM (Figure 1F, G; Table S2). Introduction of the F350L mutation therefore strongly reduced the gating-modifying properties of PcTx1 and diminished its inhibitory effect by three orders of magnitude.

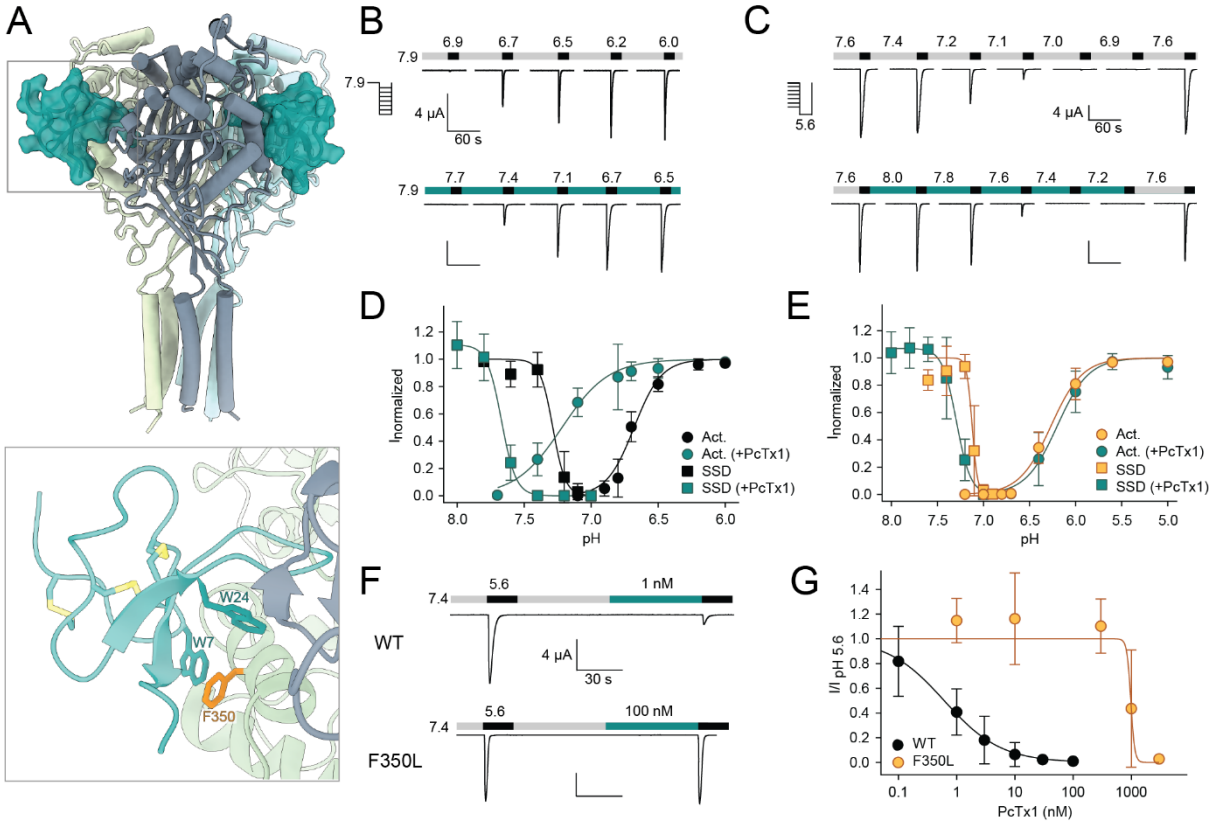

Figure 1. The F350L mutation drastically diminishes PcTx1 sensitivity of mASIC1a. (A) Model of the co-crystal structure of cASIC1a and PcTx1 (teal) binding to the extracellular domain (PDBID 4FZO). Inset shows a close up of the interaction site at the acidic pocket, including ASIC1a residue F350 (orange). (B) Representative two-electrode voltage clamp (TEVC) trace recorded from *X. laevis* oocytes showing mASIC1a WT pH activation in the absence (top) and presence (bottom) of 30 nM PcTx1. (C) Same as in B but for steady-state desensitization (SSD) of mASIC1a WT. (D) Activation and SSD curve of mASIC1a WT without (black) and with (teal) PcTx1, generated from data shown in D and E (n=6–18). (E) Same as in D but for mASIC1a F350L (n=5–14). (F) TEVC traces showing the effect of 1 nM PcTx1 on mASIC1a WT (top) and 100 nM PcTx1 on F350L (bottom) at pH 7.4. (G) PcTx1 concentration-response curve at pH 7.4 using the protocol shown in F (n=4–14). Data points in D-E and G represent mean and 95% confidence interval (95CI). All scale bars represent 4 µA and 60 s (C and D) or 30 s (F) respectively.

Conformational consequences of PcTx1 binding

The above electrophysiological characterisation provides a detailed view of how PcTx1 affects channel function, as assessed by the state of the pore. As such, it is unable to capture the extent and time course of possible conformational consequences caused by the PcTx1-ASIC1a interaction in the ECD of WT and mutant ASIC1a channels. Therefore, it remains unclear how global the toxin-induced conformational changes are and if their relative concentration dependence is similar to that of current inhibition. To overcome these shortcomings, we introduced a cysteine residue into the mASIC1a ECD at amino acid position 80 or 105 (Figure 2A) and labelled it with the environmentally sensitive AlexaFluor488 dye via a maleimide linker (Vullo, Bonifacio et al. 2017). This allowed us to monitor changes in the fluorescence signal upon channel exposure to different pH conditions and/or PcTx1 application and thus provide a proxy for ECD conformational changes at two spatially distant positions. For AlexaFluor488-labelled K105C mASIC1a (K105C*) and the K105C-F350L double mutant ASIC1a (K105C*F350L), application of pH 5.5 resulted in an inward current and a simultaneous upward

deflection of the fluorescence signal (Figure 2B, C). First, the pH dependence of the fluorescence signal was measured. For K105C*, the pH_{50} of the fluorescence signal was similar to the pH_{50_SSD}, indicating that the conformational changes tracked by fluorescent labelling likely reflect a transition related to a desensitized state (Figure S1A, B, Table S3), as reported earlier (pHs between 7.4 and 9.0 did not lead to any fluorescence changes) (Borg, Braun et al. 2020). Application of 300 nM PcTx1 at neutral pH resulted in slow upward deflection of the fluorescence, while the functional inhibition on subsequent channel activation was retained (Figure 2B; Table S4). During a 3-min washout with pH 7.4, the fluorescence signal displayed only a modest decrease from its level reached during PcTx1 application. Post-PcTx1 exposure to pH 8.4 led to an immediate return to baseline fluorescence, yet the fluorescence increased as soon as the pH was switched back to 7.4, suggesting the presence of a sustained conformational change. We observed similar effects with two other pH application protocols after PcTx1 exposure (Figure 2B bottom; S1C). The decrease in fluorescence after 3 min washout was lowest when performed at pH 7.4 (Figure 2F) and comparable between pH 8.4 and mixed washout protocols (Figure S1E, Table S5). Together, these data strongly support the notion of a distinct long-lived PcTx1-induced conformational state.

In contrast to the K105C* variant, we found that application of 300 nM PcTx1 to K105C*F350L at pH 7.4 did not elicit any fluorescence changes (Figure 2C left; Table S4). Notably, the fluorescence response curve of the K105C*F350L variant is about 0.1 pH units shifted towards more acidic pHs compared to K105C* (Figure S1B, Table S3). Taking this change into account, we applied PcTx1 at pH 7.3. Under these conditions, PcTx1 induced a similar slow-onset fluorescence signal as seen for K105C*, albeit slightly less pronounced, while the functional insensitivity of the F350L variant to PcTx1 remained (Figure 2C right, G; Table S4). The more striking difference arose in the washout: unlike in K105C*, the fluorescence signal of K105C*F350L readily returned to a level indicative of a closed *apo* state in the first 1-2 min of pH 7.4 washout (Figure 2C right, G; Table S5). These results suggest that the functional PcTx1 insensitivity of the F350L variant primarily originates from a destabilization of the PcTx1-induced conformational state rather than solely from impaired binding.

To rule out a direct interaction between the fluorophore and PcTx1 or the possibility of a local conformational change, we labelled the channel in position V80C (palm domain, Figure 2A) and characterized the pH and PcTx1 responses in the presence and absence of the F350L mutation (V80C*F350L and V80C*). When labelling this position, the direction of the fluorescence signal upon activation and desensitization was inverted (Figure 2D, E). However, application and washout of 300 nM PcTx1 at 0.3 pH units more alkaline than pH_{50} of the fluorescence signal in V80C* and V80C*F350L resulted in qualitatively similar effects as observed in K105C* and K105C*F350L, respectively (Figure 2D, E, H, I; S1D, F).

In light of the data obtained from K105C and V80C, we considered it implausible that the fluorescence changes are the result of a direct interaction between the dye and the peptide, but result from a global conformational change of the ECD upon PcTx1 binding. Given that the channel can undergo several conformational changes after PcTx1 exposure, yet retains an apparent 'memory' of PcTx1 in the fluorescence signal when switched to pH 7.4 (e.g. Figure 2B top), it also appears unlikely that PcTx1 traps the channel in a specific state that is stable even when PcTx1 is washed off. We therefore conclude that PcTx1 induces a long-lived conformational change

either via staying bound to ASIC1a without affecting the current, or through rebinding of peptides residing at or near the receptor. Importantly, this state can also be induced in the F350L variant, although it is destabilized by the mutation.

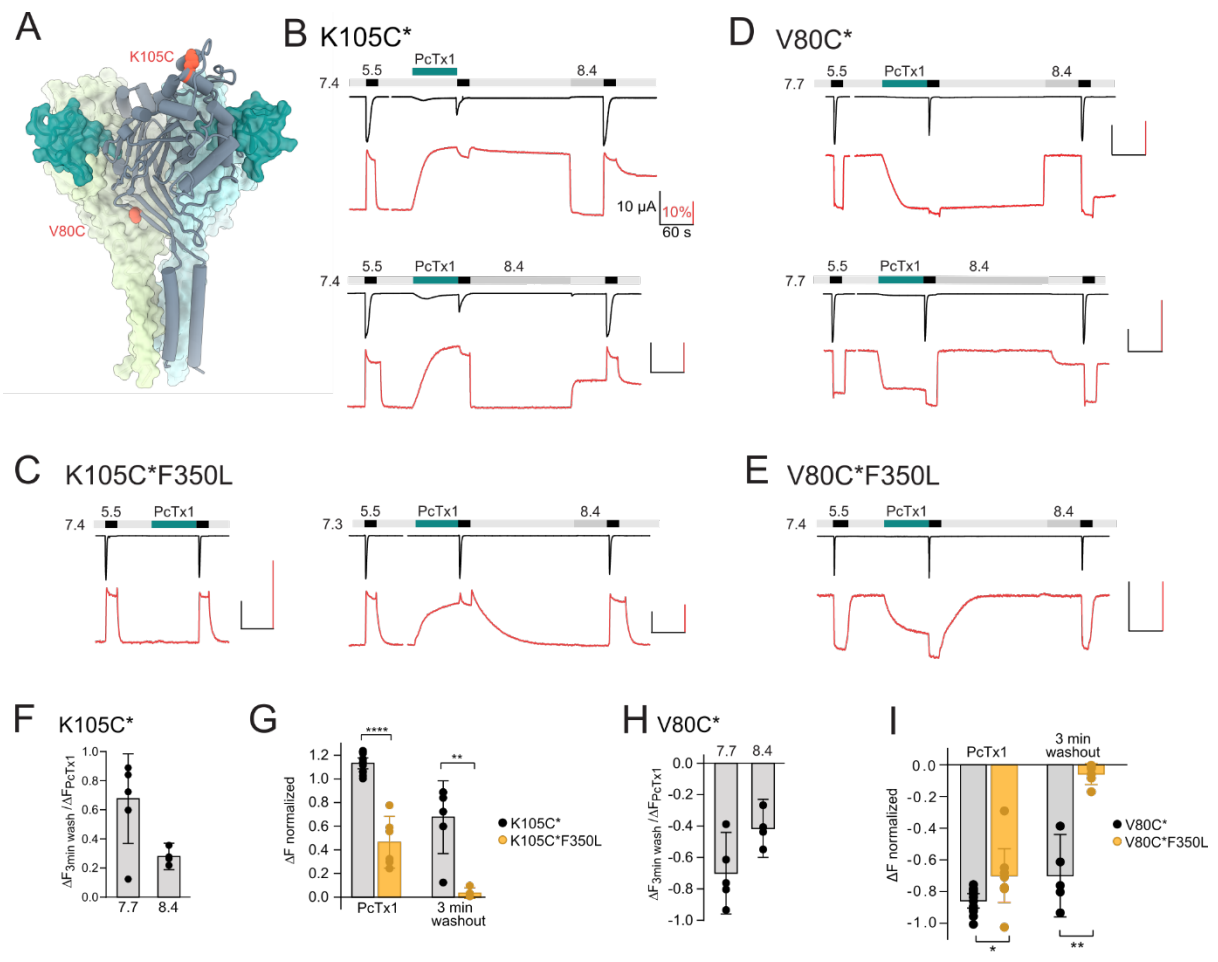

Figure 2. PcTx1 induces a distinct long-lived conformational state. (A) Structural overview of ASIC1a with residues K105 and V80, which were used to label the channel, highlighted in red. (B) Representative traces of VCF recordings of K105C* with the current in black and the fluorescence in red. PcTx1 (300 nM) was washed off for 3 min using pH 7.4 (top) or pH 8.4 (bottom). (C) Representative VCF trace of the K105C*F350L mutant showing application of 300 nM PcTx1 at pH 7.4 (left) and 7.3 (right). (D) Representative trace of a VCF recording of V80C* equivalent to the ones shown in B. (E) Same as in C but for V80C*F350L. (F) Quantitative analysis of the fluorescence signal at the end of the 3 min washout protocols shown in B relative to the fluorescence observed upon PcTx1 application. (G) Comparison of the fluorescence upon PcTx1 application and after a 3 min washout between K105C* and K150C*F350L. (H) Same analysis as in F but for V80C of data shown in D. (I) Same as in G but compared between V80C* and V80C*F350L. All scale bars are 10 µA (black vertical), 60 s (black horizontal), 10% (red). Errors are 95CI, unpaired t-Mann-Whitney test *P<0.05, **P<0.005, ****P<0.0001.

Contribution of individual F350L subunits to PcTx1 inhibition

Given the disruptive effect of the F350L mutation on PcTx1 modulation in homomeric channels (Figure 1) and heteromeric ASIC1a/2 channels (Sherwood, Lee et al. 2011, Joeres, Augustinowski et al. 2016, Cristofori-Armstrong, Saez et al. 2019), we wanted to determine the stoichiometric requirements for functional PcTx1 modulation, as well as the contribution of individual F350L-containing ASIC1a subunits to PcTx1 sensitivity. We therefore designed concatemeric ASIC1a constructs of triple WT subunits (WT/WT/WT) and constructs carrying

the F350L substitution in one, two, or all three subunits (F350L/F350L/F350L), using a previously validated construct design (Figure 3A; S2) (Lynagh, Flood et al. 2017). The pH-dependence of the WT/WT/WT and the F350L/F350L/F350L concatemer constructs showed similar pH sensitivities compared to WT and F350L, respectively (Figure 3B–E; Table S6). The number of F350L subunits determined the pH dependence of concatemeric ASIC1a constructs, but was not dependent on the relative positioning of the mutation within the concatemeric ASIC1a construct (Figure 3B–E; S3A, B; Table S6). These results provided a robust foundation to assess the effect of one, two or three F350L-bearing subunits on PcTx1 inhibition.

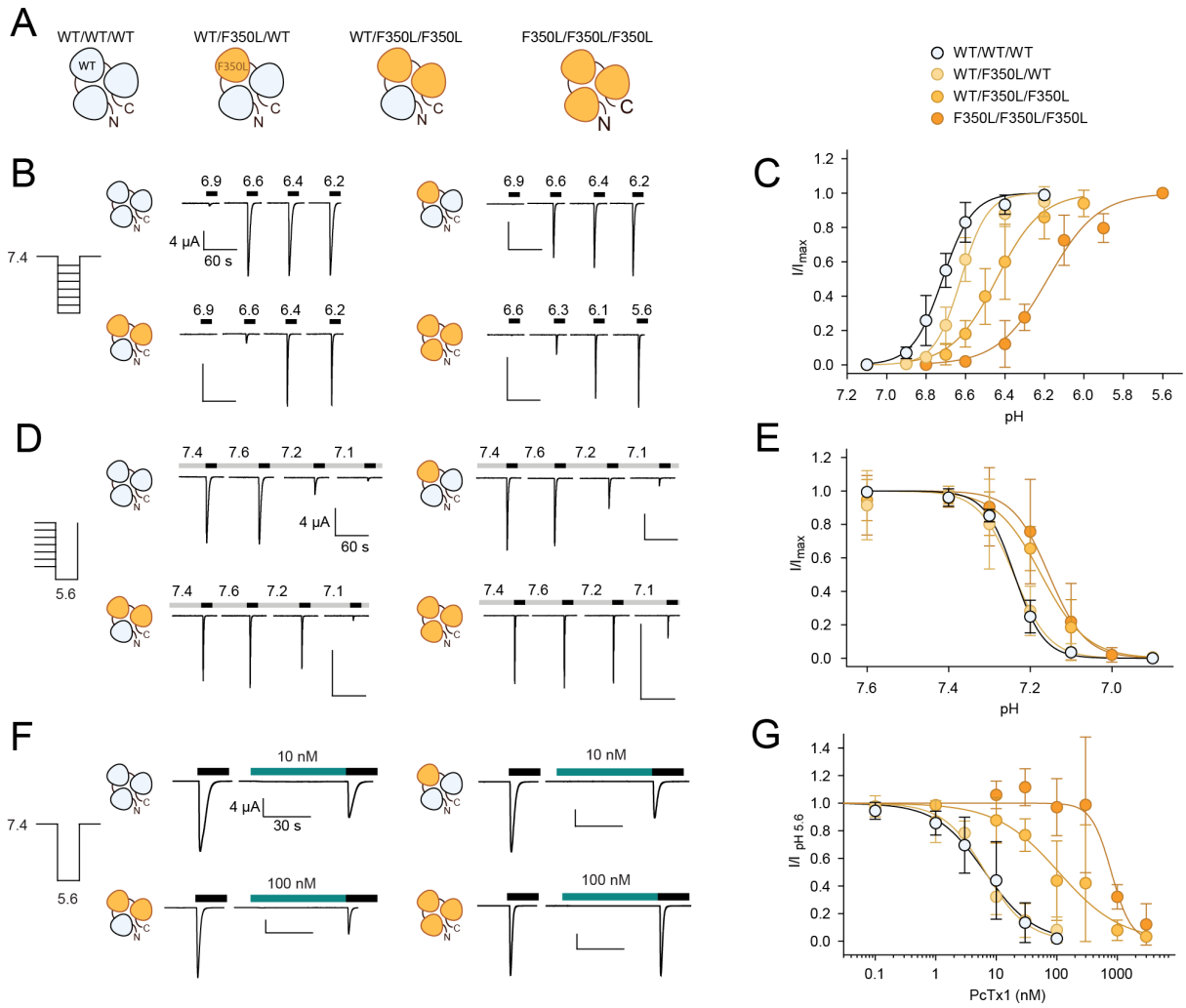

Figure 3. In concatemeric constructs, two WT subunits are sufficient for WT-like PcTx1 inhibition. (A) Schematic overview of the concatemeric constructs containing the F350L mutation in none, one, two or all three subunits. **(B)** Representative TEVC trace of activation. **(C)** Activation curve from recordings shown in B for the four different concatemeric constructs (n=7–13) **(D)** Representative TEVC trace of SSD **(E)** SSD profiles from recordings shown in D (n=4–11). **(F)** Representative TEVC trace of concentration dependent PcTx1 inhibition at pH 7.4. **(G)** PcTx1 concentration-response curves from data shown in F (n=4–11). Data points in E-G represent mean and 95CI. All scale bars are 4 µA and 30 s, respectively.

For the WT/WT/WT concatemer, pH 5.6-induced currents were inhibited by PcTx1 with an apparent IC_{50} of around 6 nM at pH 7.4, compared to an IC_{50} of 0.6 nM for WT ASIC1a (Figure 3F, G; Table S2). For the F350L/F350L/F350L concatemer, PcTx1 inhibited pH 5.6-induced currents with an apparent IC_{50} of around 800 nM, similar to the trimeric F350L ASIC1a mutant (Figure 1G; 3F, G; Table S2). This means that despite the lower PcTx1 sensitivity of the WT/WT/WT concatenated construct, the substantial decrease in PcTx1 sensitivity caused by the F350L mutation was maintained in the F350L/F350L/F350L construct. For concatenated constructs containing two F350L-bearing subunits (WT/F350L/F350L), pH 5.6-induced currents were inhibited by PcTx1 with an apparent IC_{50} around 100 nM (Figure 3F, G; S3C, Table S2). This represented a 17-fold increase in apparent IC_{50} compared to the WT/WT/WT concatemer and an 8-fold decrease compared to the F350L/F350L/F350L concatemer. Remarkably, the concatemer with only a single F350L-containing subunit (WT/F350L/WT) closely matched the PcTx1 inhibition profile observed for of the WT/WT/WT concatemer. (Figure 3F, G; S3C; Table S2).

Taken together, we demonstrate that application of PcTx1 at pH 7.4 maintains the WT-like inhibitory effect on pH 5.6 activation even if one out of three subunits contains the F350L mutation. We conclude that two WT subunits per mASIC1a trimer are sufficient to observe WT-like inhibition by PcTx1.

PcTx1-induced conformational changes in concatemeric channels

We next wanted to test if a step-wise introduction of F350L-bearing subunits would result in a difference in the stability of the PcTx1-induced ECD conformational state observed in VCF experiments. To this end, we introduced the K105C mutation in all three subunits for Alexa488-labelling, while increasing the number of F350L-containing subunits from one to two and three, respectively. We refer to subunits with WT background but labelled at K105C as WT*, while subunits labelled at K105C *and* containing the F350L mutation are designated F350L*. First, we established the pH dependence of the fluorescence signal. Overall, the pH_{50} of the fluorescence and the pH_{50_SSD} matched in all constructs and were in a similar range as the non-concatenated channels (Figure S4, Table S3). PcTx1 (300 nM) was applied 0.3 pH units above the measured $pH_{50_fluorescence}$. In the WT*/WT*/WT* concatemer, PcTx1 functionally inhibited channel activation and led to the characteristic increase in fluorescence maintained even after removal of PcTx1 from the buffer, and this was comparable to what we observed in the K105C* trimer (Figure 2B; 4A, D, E; Table S4, S5).

In WT*/F350L*/WT*concatemers, PcTx1 still had an inhibitory effect on activation, in line with the results from non-labelled constructs, and produced a robust fluorescence response (Figure 2B, D; Table S4). In this construct, a marked gradual decrease of the fluorescence signal during the 3 min washout at pH 7.4 was noticeable (Figure 4B, E; Table S5). In constructs with two F350L-containing subunits, the response of the fluorescence signal to PcTx1 was further reduced, and the fluorescence signal returned to baseline levels (indicative of a closed *apo* state) in the first 1-2 min of the pH 7.4 washout (Figure 4C–E; Table S4, S5), reminiscent of the PcTx1 effect on the non-concatemeric K105C*/F350L channel. No reliable changes in fluorescence could be detected for the F350L*/F350L*/F350L*, likely due to low expression.

In summary, our VCF experiments demonstrate that in contrast to the functional modulation, the presence of a single F350L-containing subunit is sufficient to destabilize the conformational effect introduced by PcTx1, suggesting distinct responses of the ECD and TMD to PcTx1 binding.

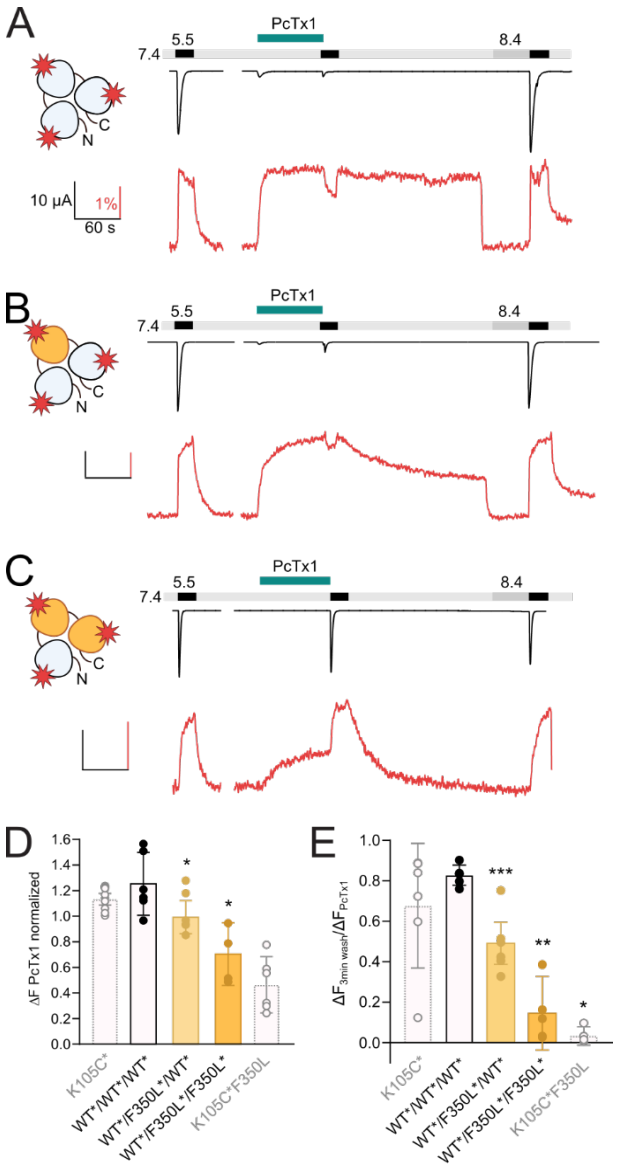

Figure 4. One F350L subunit is sufficient to destabilize the PcTx1-induced ECD conformation. (A) Representative VCF trace of 300 nM PcTx1 application to a concatemeric construct labelled at K105C* in all three subunits (red star) and subsequent washout for 3 min with pH 7.4 and 40 s pH 8.4. (B) Same as in A but one subunit carries a F350L mutation. (C) Same as in A but with two subunits carrying a F350L mutation. (D) Comparison of the PcTx1-induced change in the fluorescence signal between the different concatemeric constructs shown in A–C. Results from non-concatenated channels are indicated for comparison (shown in light grey). (E) Comparison of the fluorescence intensity after a 3 min washout relative to the intensity upon PcTx1 application. Results from non-concatenated channels are indicated for comparison (shown in light grey). All scale bars represent 10 µA (black vertical), 60 s (black horizontal), 1% (red). In D and E, errors are 95CI, unpaired t-Mann-Whitney test to left neighboring bar *P<0.05, **P<0.005, ***P<0.0005.

Discussion

The introduction of the F350L mutation in mASIC1a lowered apparent PcTx1 sensitivity by almost three orders of magnitudes compared to WT. Using concatemeric ASIC1a constructs that carry this virtually PcTx1-insensitive mutation in one, two, or all three subunits, we observed that two WT subunits are sufficient for WT-like functional modulation by PcTx1. Our VCF experiments revealed that PcTx1 introduces ECD conformational changes that are exceptionally pH-dependent and involve at least the finger and the palm domain. Binding does not appear to be limited to any specific channel state and is likely maintained beyond the application period of PcTx1. Introduction of the PcTx1-insensitive F350L mutation does not appear to prevent toxin binding, but rather diminishes the functional consequences. Importantly, F350L destabilizes the PcTx1-induced conformation even if the mutation is introduced in only a single subunit. These results highlight that ASIC1a can undergo ECD conformational rearrangements that are not necessarily reflected in channel function. Together, this emphasizes the power and resolution of protein engineering approaches and provides direct insights into the stoichiometry of the ASIC1a–PcTx1 interaction.

PcTx1-induced conformational changes

VCF experiments on K105C* and V80C* showed slow-onset PcTx1-induced fluorescence changes, indicating changes in the local environment of the fluorophore attached to the finger or palm domain, respectively. As outlined above, we deem it unlikely that the fluorescence changes are brought on by a direct interaction of PcTx1 with the fluorophore, as the fluorescence signal follows opposite directions depending on the place of labelling. This leaves the question if the conformational rearrangements reflect a transition into a different functional state or are rather related to more local PcTx1-induced conformational changes. The first possibility is supported by the phenotype of the PcTx1-induced fluorescence change, which resembles the one observed for SSD (Figure 2B; S1A), as well as the close match between the pH_{50} of the fluorescence with the pH_{50_SSD} in all variants tested here (Figure S1B,S4; table 3). The fluorescence change upon PcTx1 application could therefore reflect the transition of the channels from a closed to a SSD state upon PcTx1 application. The immediate return of the fluorescence signal to baseline during pH 8.4 application could hence be interpreted as the alkaline pH resulting in a closed rather than a SSD state, even in the presence of PcTx1. However, this hypothesis is contradicted by several observations. First, during the washout of PcTx1 in K105C* or V80C*, the sustained fluorescence signal indicates a long-lived conformational change, but the channels can already be fully activated even before the fluorescence signal fully returns to baseline (Figure 2B, D; S1G). Secondly, in the K105C*F350L and V80C*F350L variants, PcTx1 still introduces comparable conformational changes as seen for K105C* or V80C* respectively, yet no functional inhibition could be seen (Figure 2C, E, G, I), making it unlikely that channels have ever entered SSD. We therefore favour the notion that labelling allows us to track conformational changes that do not simply report on a known functional transition, but rather reflect unique ECD conformational changes induced by PcTx1.

Earlier reports have shown prolonged functional effects of PcTx1 even after washout (Escoubas, De Weille et al. 2000). Here we provide evidence for long-lived changes in protein conformation that persist even after the channels underwent several functional and conformational transitions (e.g. Figure 2B). During this washout period, PcTx1 may remain bound in a functionally non-productive conformation or the peptide could

accumulate in or at the cell membrane (Gupta, Zamanian et al. 2015) and diffuse to the binding site after perfusion of PcTx1 has been terminated. At alkaline pH, PcTx1 might unbind due to conformational changes and/or unfavourable electrostatic interaction, which would explain why different washout protocols lead to different levels in fluorescence after the same amount of time. However, it also remains plausible that the conformational state is dependent on both PcTx1 binding and a pH-dependent functional state. In any case, the ECD conformational changes are highly responsive to PcTx1, but in the presence of F350L mutations these changes are not necessarily translated to the pore, explaining why we see ECD effects without functional effects at e.g. K105C*F350L, V80C*F350L or after prolonged washout periods. We thus conclude that even subeffective PcTx1 concentrations induce a pH-dependent conformational change either via a bound or re-bound state. Such functionally silent states and conformations are often too transient or unstable to be captured in structure determination, but have previously been suggested to occur upon binding of the ASIC-modulating peptide Big dynorphin (Borg, Braun et al. 2020), as well as in other ion channels (Dahan, Dibas et al. 2004, Pless, Dibas et al. 2007, Pless and Lynch 2009, Munro, Ladefoged et al. 2019), and provide deeper insights into the dynamic conformational landscape.

The F350L mutation destabilizes a PcTx1-induced conformational state

Consistent with previous work (Sherwood, Franke et al. 2009, Saez, Deplazes et al. 2015), we observed that although the F350L mutation shifts the PcTx1 IC_{50} by about three orders of magnitude, ASIC1a is not rendered completely insensitive towards PcTx1 modulation. Reduced PcTx1-inhibition could, in part, result from the reduced pH sensitivity of the F350L variant, in line with the critical role of pH on PcTx1 modulation observed for human and rat ASIC1a (Cristofori-Armstrong, Saez et al. 2019). A mutant whose pH_{50} is shifted towards higher proton concentrations (right-shifted) would show less inhibition even if PcTx1 sensitivity was maintained. However, our VCF experiments rule out decreased pH sensitivity as the main cause for reduced PcTx1 sensitivity since we corrected for the shifts in SSD. Applied at pH 7.4, 300 nM PcTx1 (below the IC_{50} of the unlabelled F350L variant) does not lead to conformational changes, but does so at pH 7.3, although no functional effects are observed. These experiments indicate that PcTx1 interacts with F350L* and introduces conformational changes, despite the lack of functional consequences at these concentrations. This is in line with earlier results that suggested for PcTx1 to still bind to F352L hASIC1a, as pre-incubation with PcTx1 prevented the modulatory effects of Big dynorphin, a peptide that interacts with the same binding site (Sherwood and Askwith 2009, Borg, Braun et al. 2020). Similarly, experiments from ASIC1a/2a concatemers of different subunit stoichiometries suggested that PcTx1 also binds to ASIC1a-2a interfaces (Joeres, Augustinowski et al. 2016), despite the fact that ASIC2a subunits contain a Leu at the position corresponding to 350 in mASIC1a. Hence, the F350L mutation seems to diminish functional modulation by PcTx1, but not necessarily binding. Indeed, our fluorescence data indicate that the F350L mutation appears to destabilize the PcTx1-induced state, leading to faster return of the fluorescence signal to baseline levels, suggestive of a closed *apo* state.

Stoichiometry of toxin binding

Structural data have recently provided a wealth of insight into the molecular details of where and how drugs or toxins binding to ion channels. Yet these data cannot directly inform on the ligand-receptor stoichiometry

required for the full functional effect. For example, cryo-EM structures of homotetrameric KCNQ channels suggest a stoichiometric binding of the antiepileptic small-molecule drug retigabine (i.e. one drug per each of the four subunits), while functional work shows that binding of a single retigabine molecule is sufficient to elicit the full functional effect of the channel activator (Yau, Kim et al. 2018, Li, Wu et al. 2021, Li, Zhang et al. 2021). Similarly, binding of a single alpha-bungarotoxin molecule to the heteromeric nAChR pentamer is sufficient for channel inhibition, despite two molecules being present in a cryo-EM co-structure (daCosta, Free et al. 2015, Rahman, Teng et al. 2020).

To overcome limitations of heteromeric channel expression paradigms, we physically linked the three mASIC1a subunits into concatemeric constructs to simultaneously record currents and ECD conformational changes. We show that concatemers with homomeric subunit composition display comparable pH sensitivities for activation and SSD, along with similar sensitivity to PcTx1 compared to their homotrimeric counterparts. Functionally, we demonstrate that two WT ASIC1a subunits are sufficient for WT-like PcTx1 sensitivity at physiological pH. Our VCF results, however, revealed that a single F350L subunit is sufficient to destabilize the PcTx1-induced conformation, which then further decreases in a stepwise manner in channels containing two or three mutant subunits.

As established above, ECD conformational changes are likely more sensitive to PcTx1 than the changes that are translated to the pore. It is therefore not surprising that VCF experiments revealed the destabilizing effect of one F350L-containing subunit on the PcTx1-induced conformational state although functional differences are only observed when two F350L-containing subunits are present. We consequently propose that conformational changes of the ECD are partially decoupled from the TMD and that the ECD adopts different conformations depending on how many PcTx1 molecules are bound, while the pore (or the coupling to it) translates to closed channels only in conformations associated with binding of two or more peptides (Figure 5). Such a scenario would explain why introduction of just a single F350L mutation is sufficient to destabilize the PcTx1-induced conformational state in the ECD, while the functional state of the pore still displays WT-like behaviour and is only affected once two (or more) subunits are rendered PcTx1 insensitive.

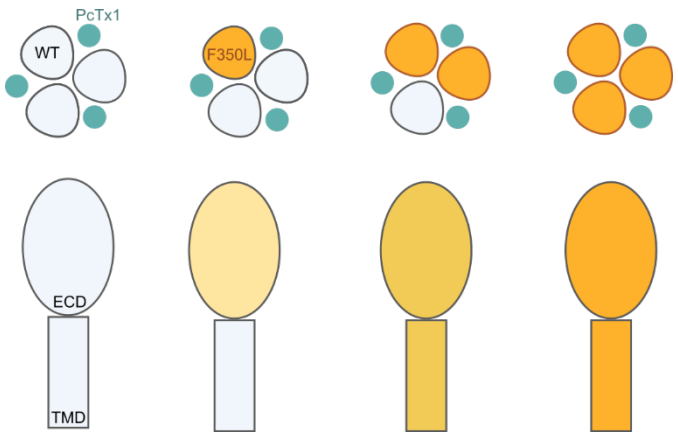

Figure 5. Schematic representation of divergent functional and conformational effects of PcTx1 modulation. (Top) Representation of the three mASIC1a subunit with the F350L mutation in 0–3 subunits and PcTx1 in teal. **(Bottom)** Simple illustration of mASIC1a and the effect of increasing numbers of F350L-bearing subunits on the PcTx1 induced changes to ECD and TMD. Shades of yellow illustrate the increasing destabilization of the PcTx1 ECD conformation and the decreasing inhibitory effect on the pore . In channels with only one F350L subunit, only the PcTx1-induced conformational state of the ECD is affected by PcTx1 binding.

Conclusions

The conformational landscape of ion channels is likely to far exceed the conformations uncovered by structural or functional studies, as it is often challenging to capture such states in compelling ways. By combining concatemeric construct design with voltage-clamp fluorometry, we provide insight into functionally-silent conformational changes of the mASIC1a ECD during PcTx1 modulation and assess the contribution of individual subunits to the overall conformational state and on the functional state of the pore. To our knowledge, the work presented here constitutes the first use of concatemeric multisubunit assemblies engineered for VCF recordings, thus offering the potential to label a defined subset of subunits to unveil potential asymmetric gating and binding events, such as those proposed for a variety of ligand-gated ion channels (Jasti, Furukawa et al. 2007, Baconguis and Gouaux 2012, Mowrey, Cheng et al. 2013, Zhu, Noviello et al. 2018, Guros, Balijepalli et al. 2020, Zhang, Dijkman et al. 2021).

Acknowledgments

We acknowledge funding from the Lundbeck Foundation (R303-2018-3030 to SAH and R313-2019-571 to SAP) and the European Union's Horizon 2020 research and innovation program under the Marie Skłodowska-Curie grant agreement No 834274 (to SAH). We thank Assist. Prof. Han Chow Chua for comments on the manuscript.

Materials and Methods

Molecular biology.

The complementary DNA (cDNA) encoding mouse ASIC1a (mASIC1a) was used as previously described (Lynagh, Flood et al. 2017). Site-directed mutagenesis was performed using PfuUltraII Fusion polymerase (Agilent) and custom DNA mutagenesis primers (Eurofins Genomics). All sequences were confirmed by sequencing of the full coding frame (Eurofins Genomics or Macrogen). cDNAs were linearized with EcoRI and capped cRNA was transcribed with the Ambion mMESSAGE mMACHINE SP6 kit (Thermo Fisher Scientific).

Concatemer design

Mouse ASIC1a concatemeric constructs were generated as described before (Lynagh, Flood et al. 2017). Briefly, the concatemeric mASIC1a constructs were generated by cloning out the mASIC1a insert from the pSP64 vector using forward and reverse primers containing additional HindIII and SalI, SalI and BamHI or BamHI and SacI sequences, respectively (Figure S2). This generated three distinct inserts, *a*, *b* and *c*, which were gel-purified using the Gel/PCR DNA fragment kit (Geneaid). The inserts were digested with their respective restriction enzymes, insert *a*: HindIII and SalI, insert *b*: SalI and BamHI, and insert *c*: BamHI and SacI. Insert *a* was ligated into the empty pSP64 vector (Promega) double-digested with HindIII and SalI. The resulting vector was then double-digested with SalI and BamHI to insert segment *b* in similar way. The *a-b* plasmid was then double-digested using BamHI and SacI and segment *c* was ligated into it. This yielded the final "*a-b-c*" mASIC1a concatemer. From this construct, WT inserts were replaced by mASIC1a inserts containing amino acid substitutions generated using the same primers and restriction sites. Full concatemer sequences were confirmed using primers recognizing the unique restriction sites.

Electrophysiological recordings. Oocytes were surgically removed from adult female *Xenopus laevis* and prepared as previously described (Lynagh, Flood et al. 2017). Oocytes were injected with 0.1 to 10 ng cRNA of mASIC1a (volumes between 9 and 50 nL) and incubated for 1–4 days at 18 °C in Leibovitz's L-15 medium (Gibco), supplemented with 3 mM L-glutamine, 2.5 mg/ml gentamycin and 15 mM HEPES adjusted to pH 7.6. Typically, larger amounts of mutant mASIC1a cRNA were injected compared to WT mASIC1a. For electrophysiological recordings, oocytes were transferred to a recording chamber (Dahan, Dibas et al. 2004), continuously perfused (2.5 mL/min) with buffer containing (in mM): 96 NaCl, 2 KCl, 1.8 $BaCl_2$, 2 $MgCl_2$, and 5 HEPES, pH adjusted by NaOH or HCl. Solutions exchange was achieved using a gravity-driven 8-line automated perfusion system operated by a ValveBank module (AutoMate Scientific). In experiments where PcTx1 was used, all solutions were supplemented with 0.05% bovine serum albumin (≥ 98% essentially fatty acid-free, Sigma Aldrich). Currents were recorded using microelectrodes (borosilicate capillaries 1.2 mm OD, 0.94 mm ID, Harvard Apparatus), backfilled with 3 M KCl (0.3–1.5 MΩ) and an OC-725C amplifier (Warner Instruments). The current signal was acquired at 500 Hz, filtered by a 50-60 Hz noise eliminator (Hum Bug, Quest Scientific)

and digitized using an Axon™ Digidata® 1550 Data Acquisition System and the pClamp (10.5.1.0) software (Molecular Devices). The current signal was further digitally filtered at 2.8 Hz using an 8-pole Bessel low-pass filter prior to analysis. Displayed current traces have been subjected to additional 50× data reduction.

Synthetic PcTx1 was obtained from Alomone Labs (>95 % purity). PcTx1 stock solutions were prepared in MilliQ (18.2 MΩ resistivity). Peptide stock solutions were stored at -20 °C. Prior to recording, the peptide was diluted to the desired concentration in recording solution.

Concentration-response relationships of mASIC1a activation were determined by 20 s applications of solutions with decreasing pH-values. Between each 20 s application, the oocytes were left to recover for at least 1 min in pH 7.4 solution (unless stated otherwise). The currents elicited by the 20 s application of acidic pH were normalized to the largest current size for each of individual oocyte tested. Steady-state desensitization (SSD) concentration-response relationships were determined by exposing ASIC1a expressing oocytes to a 20 s application of pH 5.6 (unless stated otherwise), while decreasing the resting pH in between applications of pH 5.6. In order to ensure that the observed current desensitization was not due to general current run-down, a final application of pH 5.6 was performed after a 2 min resting period at a resting pH that resulted in saturating current responses. Traces were used for further analysis only if the final pH 5.6 application resulted in currents that were ≥ 80 % of the same resting pH prior to the SSD protocol. For testing of the effect of PcTx1 on the ASIC1a current response, channels were activated by 20 s application of pH 5.6. Hereafter the pH solution returned to resting pH to allow channel recovery. PcTx1 was then applied at the desired pH for 1 min prior to a 20 s application of pH 5.6.

Voltage-clamp fluorometry. For voltage-clamp fluorometry (VCF), 5-20 ng of mASIC1a mRNA or 50 ng for concatemeric constructs were injected into oocytes which were then incubated for 2–7 days. On the day of the recording, oocytes were labeled by incubating them for 30 min with 10 µM AlexaFlour 488 C5-maleimide (Thermo Fisher Scientific) at room temperature in OR2 solution containing (in mM) 82.5 NaCl, 2 KCl, 1 $MgCl_2$, pH 7.4, subsequently washed twice with OR2, and stored in the dark until further use. Concatemeric constructs were kept in the dark for several hours, as it tended to reduce background fluorescence. VCF recordings were done as previously described (Borg, Braun et al. 2020) using an inverse microscope (IX73 with LUMPlanFL N 40x, Olympus) an Olympus TH4-200 halogen lamp as light source and using a standard GFP filter-set (Olympus). The emission was detected using a P25PC-19 photomultiplier tube (Sens-Tech) and photon-to-voltage converter (IonOptix). Current and fluorescence signals were acquired, filtered, digitized and digitally filtered as described for the other electrophysiology recordings.

For SSD and pH-dependent fluorescence measurements, running buffer at pH 7.6 was used and labelled channels were activated for 20 s using pH 6.0, washed for 1 min with pH 7.6 buffer, exposed for 1 min to buffer at conditioning pH and then directly activated again (Figure S1A). Control activations at pH 6.0 were conducted between each SSD measurement. For PcTx1 responses, running buffer at 0.3 pH units above the established

$pH_{50_fluorescence}$ was used, unless stated otherwise. First channels were activated for 20 s with pH 5.5, washed for 60 s with running buffer before applying 300 nM PcTx1. Washout protocols either included 3 min exposure to running buffer, pH 8.4 buffer, or a mix of the two (20 s running buffer, 60 s pH 8.4, 40 s running buffer, 60s pH 8.4).

Surface protein purification. Oocyte surface proteins were purified using the Pierce Cell Surface Protein Isolation Kit (Thermo Fisher Scientific), modified here for oocytes as previously described (Lynagh, Flood et al. 2017). In brief, 30 oocytes were injected with RNA of a single mASIC1a construct. After two days of incubation the oocytes were washed with phosphate buffered saline (PBS) and incubated for 25 min at room temperature with sulfo-NHS-SS-biotin. Hereafter, the reaction was quenched and oocytes were washed with PBS. The oocytes were lysed, centrifuged, and the clarified supernatant was transferred to a spin column containing equilibrated NeutrAvidin Agarose and incubated for 1 hour at room temperature under gentle agitation. The flow-through was discarded and the NeutrAvidin Agarose was washed and centrifuged. The wash procedure was repeated for a total of three times. Prior to elution, 200 µL SDS-PAGE sample buffer containing 50 mM dithiothreitol (DTT) was added and the column was incubated for 60 min at room temperature under agitation. The protein was then eluted by centrifugation. The concentration of protein was determined using the NanoDrop One^{C} UV-Vis spectrophotometer and the samples were stored at -20 °C.

Western blotting. Oocyte surface protein samples were denatured for 5 min at 90 °C in LDS sample buffer containing reducing agent (50 mM DTT) (NuPAGE®, Thermo Fisher Scientific). Protein samples (10-120 µg, dependent on the construct in order to get approximately equal band intensity), Novex Sharp pre-stained standard (Thermo Fisher Scientific) were separated by SDS-PAGE using a 4-12 % Bis-Tris protein gel (NuPAGE®, Thermo Fisher Scientific). Protein bands were transferred to a polyvinylidene difluoride (PVDF) membrane (0.45 µm, Thermo Fisher Scientific) in transfer buffer (NuPAGE®, Thermo Fisher) containing 10 % methanol (MeOH). After transfer, the PVDF membrane was rinsed with tris buffered saline 0.1% tween (TBST) and subsequently blocked with 0.5 % non-fat dried milk (AppliChem) in TBST using the Snap i.d.® 2.0 Protein Detection System (Millipore). The blot was then incubated for 10 min at room temperature with a 1:1000 dilution of rabbit polyclonal anti-ASIC1a antibody (OSR00097W, Thermo Fisher Scientific) in blocking buffer followed by 10 min incubation at room temperature with goat anti-rabbit IgG/horseradish peroxidase-conjugate (1:10,000 dilution of 1 mg/mL stock in blocking buffer) (A16110, Thermo Fisher Scientific). The blot was developed using enhanced chemoluminescence detection reagents (Pierce™ ECL Western Blotting Substrate, Thermo Fisher Scientific) and visualized using a PXi Touch Gel Imaging System (Syngene).

Data analysis. Data analyses were performed in Prism (8.0) (GraphPad Software). Fluorescence baseline was adjusted for all fluorescence traces before analysis. For proton concentration-response data, peak amplitudes

were normalized to control activations, plotted as a function of pH, and fitted with the Hill equation constrained at min = 0 (and max = 1 for TEVC data) for each recording. The resulting EC_{50} and Hill values were averaged to give the reported means ± 95CI in the tables. For PcTx1 inhibition experiments, current responses after PcTx1 treatment were normalized to the current responses without PcTx1 incubation for each oocyte. The average data for the different PcTx1 concentrations were fitted using a Hill-equation constrained at min = 0 and max = 1. For display in figures, a single fit to the average normalized responses (± 95CI) is shown. The change in fluorescence upon PcTx1 application was normalized to the neighbouring pH 5.5 application. Washout of PcTx1 in VCF experiments was reported as the level of fluorescence under running buffer at the end of the 3 min washout relative to the PcTx1-induce fluorescence change. Fluorescence signal intensity was reported as percentage change relative to the baseline fluorescence level.

All bar diagrams and summarized data points are presented as mean ± 95CI unless stated otherwise and number of replicates (n) represent individual experimental oocytes. Results were obtained from at least two batches of oocytes. An unpaired t-Mann-Whitney test was used to compare two groups. Multiple comparisons in Figure S1E and F were made with one-way analysis of variance with Dunnett's comparison to a control value (i.e. washout using running buffer). A significance level of $p < 0.05$ was applied for all analyses. All graphs and illustrations were made in Prism (8.0) (GraphPad Software) and Illustrator CC (Adobe), structure rendering was done using ChimeraX (Pettersen, Goddard et al. 2021).

References

Baconguis, I., C. J. Bohlen, A. Goehring, D. Julius and E. Gouaux (2014). "X-ray structure of acid-sensing ion channel 1-snake toxin complex reveals open state of a Na(+)-selective channel." Cell **156**(4): 717-729.

Baconguis, I. and E. Gouaux (2012). "Structural plasticity and dynamic selectivity of acid-sensing ion channel-spider toxin complexes." Nature **489**(7416): 400-405.

Borg, C. B., N. Braun, S. A. Heusser, Y. Bay, D. Weis, I. Galleano, C. Lund, W. Tian, L. M. Haugaard-Kedstrom, E. P. Bennett, T. Lynagh, K. Stromgaard, J. Andersen and S. A. Pless (2020). "Mechanism and site of action of big dynorphin on ASIC1a." Proc Natl Acad Sci U S A **117**(13): 7447-7454.

Chassagnon, I. R., C. A. McCarthy, Y. K. Chin, S. S. Pineda, A. Keramidas, M. Mobli, V. Pham, T. M. De Silva, J. W. Lynch, R. E. Widdop, L. D. Rash and G. F. King (2017). "Potent neuroprotection after stroke afforded by a double-knot spider-venom peptide that inhibits acid-sensing ion channel 1a." Proc Natl Acad Sci U S A **114**(14): 3750-3755.

Chen, X., H. Kalbacher and S. Grunder (2005). "The tarantula toxin psalmotoxin 1 inhibits acid-sensing ion channel (ASIC) 1a by increasing its apparent H+ affinity." J Gen Physiol **126**(1): 71-79.

Chen, X., H. Kalbacher and S. Grunder (2006). "Interaction of acid-sensing ion channel (ASIC) 1 with the tarantula toxin psalmotoxin 1 is state dependent." J Gen Physiol **127**(3): 267-276.

Cristofori-Armstrong, B. and L. D. Rash (2017). "Acid-sensing ion channel (ASIC) structure and function: Insights from spider, snake and sea anemone venoms." Neuropharmacology **127**: 173-184.

Cristofori-Armstrong, B., N. J. Saez, I. R. Chassagnon, G. F. King and L. D. Rash (2019). "The modulation of acid-sensing ion channel 1 by PcTx1 is pH-, subtype- and species-dependent: Importance of interactions at the channel subunit interface and potential for engineering selective analogues." Biochem Pharmacol **163**: 381-390.

daCosta, C. J. B., C. R. Free and S. M. Sine (2015). "Stoichiometry for α-bungarotoxin block of α7 acetylcholine receptors." Nat Commun **6**(1): 8057.

Dahan, D. S., M. I. Dibas, E. J. Petersson, V. C. Auyeung, B. Chanda, F. Bezanilla, D. A. Dougherty and H. A. Lester (2004). "A fluorophore attached to nicotinic acetylcholine receptor beta M2 detects productive binding of agonist to the alpha delta site." Proc Natl Acad Sci U S A **101**(27): 10195-10200.

Dawson, R. J., J. Benz, P. Stohler, T. Tetaz, C. Joseph, S. Huber, G. Schmid, D. Hugin, P. Pflimlin, G. Trube, M. G. Rudolph, M. Hennig and A. Ruf (2012). "Structure of the acid-sensing ion channel 1 in complex with the gating modifier Psalmotoxin 1." Nat Commun **3**: 936.

Du, J., L. R. Reznikov, M. P. Price, X.-m. Zha, Y. Lu, T. O. Moninger, J. A. Wemmie and M. J. Welsh (2014). "Protons are a neurotransmitter that regulates synaptic plasticity in the lateral amygdala." Proc Natl Acad Sci USA **111**(24): 8961-8966.

Escoubas, P., J. R. De Weille, A. Lecoq, S. Diochot, R. Waldmann, G. Champigny, D. Moinier, A. Menez and M. Lazdunski (2000). "Isolation of a tarantula toxin specific for a class of proton-gated Na+ channels." J Biol Chem **275**(33): 25116-25121.

Gründer, S. (2020). Acid-Sensing Ion Channels The Oxford Handbook of Neuronal Ion Channels. A. Bhattacharjee, Oxford University Press**:** 1-56.

Gupta, K., M. Zamanian, C. Bae, M. Milescu, D. Krepkiy, D. C. Tilley, J. T. Sack, V. Yarov-Yarovoy, J. I. Kim and K. J. Swartz (2015). "Tarantula toxins use common surfaces for interacting with Kv and ASIC ion channels." Elife **4**.

Guros, N. B., A. Balijepalli and J. B. Klauda (2020). "Microsecond-timescale simulations suggest 5-HT-mediated preactivation of the 5-HT3A serotonin receptor." Proc Natl Acad Sci U S A **117**(1): 405-414.

Jasti, J., H. Furukawa, E. B. Gonzales and E. Gouaux (2007). "Structure of acid-sensing ion channel 1 at 1.9 A resolution and low pH." Nature **449**(7160): 316-323.

Joeres, N., K. Augustinowski, A. Neuhof, M. Assmann and S. Grunder (2016). "Functional and pharmacological characterization of two different ASIC1a/2a heteromers reveals their sensitivity to the spider toxin PcTx1." Sci Rep **6**: 27647.

Kellenberger, S. and L. Schild (2015). "International Union of Basic and Clinical Pharmacology. XCI. structure, function, and pharmacology of acid-sensing ion channels and the epithelial Na+ channel." Pharmacol Rev **67**(1): 1-35.

Li, T., K. Wu, Z. L. Yue, Y. F. Wang, F. Zhang and H. Z. Shen (2021). "Structural Basis for the Modulation of Human KCNQ4 by Small-Molecule Drugs." Molecular Cell **81**(1): 25-+.

Li, X. X., Q. S. Zhang, P. P. Guo, J. Fu, L. H. Mei, D. S. Lv, J. Q. Wang, D. W. Lai, S. Ye, H. Y. Yang and J. T. Guo (2021). "Molecular basis for ligand activation of the human KCNQ2 channel." Cell Research **31**(1): 52-61.

Lynagh, T., E. Flood, C. Boiteux, M. Wulf, V. V. Komnatnyy, J. M. Colding, T. W. Allen and S. A. Pless (2017). "A selectivity filter at the intracellular end of the acid-sensing ion channel pore." eLife **6**.

Mowrey, D., M. H. Cheng, L. T. Liu, D. Willenbring, X. Lu, T. Wymore, Y. Xu and P. Tang (2013). "Asymmetric ligand binding facilitates conformational transitions in pentameric ligand-gated ion channels." J Am Chem Soc **135**(6): 2172-2180.

Munro, L., L. K. Ladefoged, V. Padmanathan, S. Andersen, B. Schiott and A. S. Kristensen (2019). "Conformational Changes in the 5-HT3A Receptor Extracellular Domain Measured by Voltage-Clamp Fluorometry." Mol Pharmacol **96**(6): 720-734.

Pettersen, E. F., T. D. Goddard, C. C. Huang, E. C. Meng, G. S. Couch, T. I. Croll, J. H. Morris and T. E. Ferrin (2021). "UCSF ChimeraX: Structure visualization for researchers, educators, and developers." Protein Sci **30**(1): 70-82.

Pless, S. A., M. I. Dibas, H. A. Lester and J. W. Lynch (2007). "Conformational variability of the glycine receptor M2 domain in response to activation by different agonists." J Biol Chem **282**(49): 36057-36067.

Pless, S. A. and J. W. Lynch (2009). "Ligand-specific conformational changes in the alpha1 glycine receptor ligand-binding domain." J Biol Chem **284**(23): 15847-15856.

Qiang, M., X. Dong, Z. Zha, X. K. Zuo, X. L. Song, L. Zhao, C. Yuan, C. Huang, P. Tao, Q. Hu, W. G. Li, W. Hu, J. Li, Y. Nie, D. Buratto, F. Zonta, P. Ma, Z. Yu, L. Liu, Y. Zhang, B. Yang, J. Xie, T. L. Xu, Z. Qu, G. Yang and R. A. Lerner (2018). "Selection of an ASIC1a-blocking combinatorial antibody that protects cells from ischemic death." Proc Natl Acad Sci U S A **115**(32): E7469-E7477.

Rahman, M. M., J. Teng, B. T. Worrell, C. M. Noviello, M. Lee, A. Karlin, M. H. B. Stowell and R. E. Hibbs (2020). "Structure of the Native Muscle-type Nicotinic Receptor and Inhibition by Snake Venom Toxins." Neuron **106**(6): 952-962.e955.

Saez, N. J., E. Deplazes, B. Cristofori-Armstrong, I. R. Chassagnon, X. Lin, M. Mobli, A. E. Mark, L. D. Rash and G. F. King (2015). "Molecular dynamics and functional studies define a hot spot of crystal contacts essential for PcTx1 inhibition of acid-sensing ion channel 1a." Br J Pharmacol **172**(20): 4985-4995.

Sherwood, T., R. Franke, S. Conneely, J. Joyner, P. Arumugan and C. Askwith (2009). "Identification of protein domains that control proton and calcium sensitivity of ASIC1a." J Biol Chem **284**(41): 27899-27907.

Sherwood, T. W. and C. C. Askwith (2009). "Dynorphin opioid peptides enhance acid-sensing ion channel 1a activity and acidosis-induced neuronal death." J Neurosci **29**(45): 14371-14380.

Sherwood, T. W., K. G. Lee, M. G. Gormley and C. C. Askwith (2011). "Heteromeric acid-sensing ion channels (ASICs) composed of ASIC2b and ASIC1a display novel channel properties and contribute to acidosis-induced neuronal death." J Neurosci **31**(26): 9723-9734.

Vullo, S., G. Bonifacio, S. Roy, N. Johner, S. Berneche and S. Kellenberger (2017). "Conformational dynamics and role of the acidic pocket in ASIC pH-dependent gating." Proc Natl Acad Sci U S A **114**(14): 3768-3773.

Wemmie, J. A., J. Chen, C. C. Askwith, A. M. Hruska-Hageman, M. P. Price, B. C. Nolan, P. G. Yoder, E. Lamani, T. Hoshi, J. H. Freeman, Jr. and M. J. Welsh (2002). "The acid-activated ion channel ASIC contributes to synaptic plasticity, learning, and memory." Neuron **34**(3): 463-477.

Wemmie, J. A., R. J. Taugher and C. J. Kreple (2013). "Acid-sensing ion channels in pain and disease." Nat Rev Neurosci **14**(7): 461-471.

Wu, Y., Z. Chen and C. M. Canessa (2019). "A valve-like mechanism controls desensitization of functional mammalian isoforms of acid-sensing ion channels." Elife **8**.

Xiong, Z. G., X. M. Zhu, X. P. Chu, M. Minami, J. Hey, W. L. Wei, J. F. MacDonald, J. A. Wemmie, M. P. Price, M. J. Welsh and R. P. Simon (2004). "Neuroprotection in ischemia: blocking calcium-permeable acid-sensing ion channels." Cell **118**(6): 687-698.

Yau, M. C., R. Y. Kim, C. K. Wang, J. R. Li, T. Ammar, R. Y. Yang, S. A. Pless and H. T. Kurata (2018). "One drug-sensitive subunit is sufficient for a near-maximal retigabine effect in KCNQ channels." J. Gen Physiol **150**(10): 1421-1431.

Zhang, Y., P. M. Dijkman, R. Zou, M. Zandl-Lang, R. M. Sanchez, L. Eckhardt-Strelau, H. Kofeler, H. Vogel, S. Yuan and M. Kudryashev (2021). "Asymmetric opening of the homopentameric 5-HT3A serotonin receptor in lipid bilayers." Nat Commun **12**(1): 1074.

Zhu, S., C. M. Noviello, J. Teng, R. M. Walsh, Jr., J. J. Kim and R. E. Hibbs (2018). "Structure of a human synaptic GABAA receptor." Nature **559**(7712): 67-72.